Dynamic eigen-modes in magnetic stripes and dots



2003 J. Phys.: Condens. Matter 15 S2575

(http://iopscience.iop.org/0953-8984/15/34/307)

INSTITUTE OF PHYSICS PUBLISHING JOURNAL OF PHYSICS: CONDENSED MATTER

J. Phys.: Condens. Matter **15** (2003) S2575–S2598 PII: S0953-8984(03)65312-9

# Dynamic eigen-modes in magnetic stripes and dots

**S O Demokritov**

Department of Physics, Kaiserslautern University of Technology, 67663 Kaiserslautern, Germany

Received 24 June 2003
Published 15 August 2003
Online at stacks.iop.org/JPhysCM/15/S2575

**Abstract**

Eigen-modes of unconfined ferromagnetic media (spin waves) were introduced by Bloch to explain the thermodynamics of ferromagnets. In this paper we analyse the eigen-modes of laterally confined magnetic structures. The quantization of eigen-modes due to the finite size of the structures as well as their localization due to the recently discovered spin wave wells effect will be considered in detail. A general description of magnetic dynamic eigen-modes in media with a strongly nonuniform internal field, important for confined structures, will be presented. Pictorial effects of spin wave propagation, reflection and tunnelling caused by field inhomogeneity will be demonstrated and discussed.

## 1. Introduction

The concept of lowest lying dynamic eigen-modes of unconfined magnetic media called spin waves was introduced by Bloch in 1930 [1]. Early experimental evidence for the existence of spin waves came from measurements of thermodynamic properties, but the first direct observation was made by means of ferromagnetic resonance (FMR) [2] and the next by means of light scattering [3]. In quantum mechanical approaches the spin wave quanta, magnons, are similar to quanta of light, photons, or those of acoustic waves, phonons. However, as will be discussed in this paper, spin waves, or magnons, have a very characteristic dispersion. Unlike phonons or photons, they usually have a gap in their spectrum which depends on the applied magnetic field and, thus, can be manipulated by a researcher.

An infinitely propagating plane spin wave is not an eigen-mode of a small magnetic element due to confinement effects. Small magnetic elements made by patterning of magnetic films have recently received much attention from the scientific community, since they are a basic part of, for example, magnetic sensors in magnetic reading heads and in magnetic random access memory (MRAM). The basic knowledge on dynamic eigen-modes of patterned magnetic structures is mandatory for the understanding of dynamic processes, in particular those involved in fast switching of the magnetization direction.

Magnetic systems possess a peculiarity, unusual for other systems: since the elements are magnetized, the magnetization generates magnetic stray fields inside and outside the elements. These strongly inhomogeneous fields determine the intrinsic inhomogeneity of the internal field

  

distribution within the element. Therefore understanding of magnetization dynamics in small elements demands explicit consideration of spatially varying internal fields, which, on one hand, makes the problem more complex and, on the other hand, results in new phenomena, such as the localization of modes in certain regions within the element.

The outline of the paper is as follows. After a short description of the preparation of patterned magnetic structures and presentation of typical examples of such systems in section 2, we will analyse dynamic eigen-modes in inhomogeneous media. In particular, spin wave quantization caused by the lateral confinement in small elements will be addressed in section 3. In the same section the analogy between spin wave propagation and that of a quantum mechanical particle will be considered. A very important tool for investigation of magnetic dynamics is the Brillouin light scattering (BLS) technique, which will be discussed in section 4. Section 5 is devoted to space and time resolved BLS. The advantages of BLS will be demonstrated in section 6 using the example of the quantization of spin waves in axially magnetized magnetic stripes. An experimental study of spin waves in strongly inhomogeneous fields, demonstrating spin wave propagation, reflection and tunnelling through a potential barrier, will be presented in section 7. The appearance of localization effects of spin waves in small elements due to the inhomogeneity of the internal field, an effect which is reminiscent of the quantum well effect in quantum mechanics, will be discussed in detail in section 8. Section 9 concludes this paper.

## 2. Magnetic patterning

In the past decade remarkable progress in the fabrication of high quality patterned magnetic structures with lateral extents on the micrometre, sub-micrometre and nanometre length scales has been made [4–6].

Lateral magnetic structures are conveniently fabricated from different magnetic films using lithographic patterning procedures. Patterned systems based on permalloy (Fe–Ni alloy) have the utmost importance in fundamental studies. The low coercive field, small constants of the intrinsic magnetocrystalline anisotropy and magnetostriction, narrow lines of FMR and light scattering facilitate the observation of sometimes minute effects caused by, e.g., the spin wave well effect. However, patterned structures made of Co-based alloys with their higher coercive fields are more important for information technology applications, such as in MRAM.

It is usually extremely difficult to study a single magnetic element, since this challenges the sensitivity of the measurement set-up [7]. To avoid this problem the elements under investigation are usually assembled in arrays. The patterns determining the array layout can be numerous [8]. However, systems comprising elements with one restricted lateral dimension, called ‘stripes’, are of particular importance. As will be seen below, applying the external field either along or perpendicular to the stripe axis, one can study different confinement effects. Similarly, elements with two restricted dimensions are called circular ‘dots’ or rectangular ‘elements’ following the usual conventions, although, as will be one of the subjects of this paper, no real reduction of dimensionality occurs since both in ‘stripes’ and ‘dots’ the magnetization is not constant over each magnetic object along a direction of restricted dimension.

The patterning process is most often performed by means of electron beam lithography (EBL) [9–11] or x-ray lithography (XRL) [12], followed by ion beam etching for pattern transfer.

Figure 1 shows scanning electron micrographs of dense arrays of permalloy rectangular elements, circular dots and stripes, demonstrating the quality which can be achieved by those techniques.

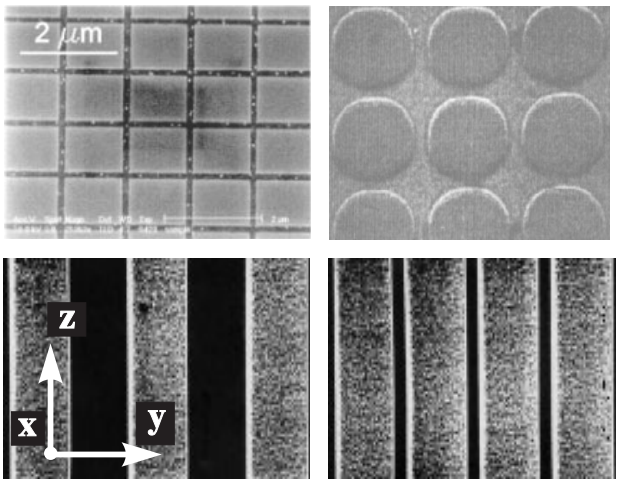


**Figure 1.** Scanning electron micrographs of permalloy arrays of rectangular elements obtained by EBL and also circular dots and long stripes with different distances between the stripes obtained by XRL. The Cartesian coordinate system used later in the text is shown as well.

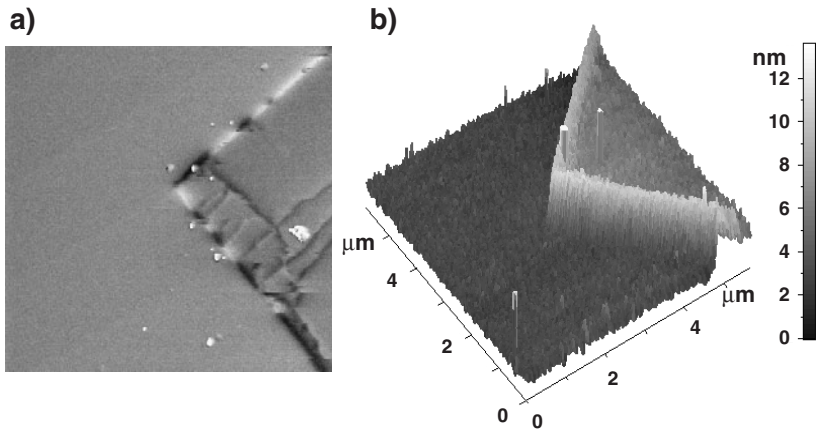


**Figure 2.** (a) A magnetic force microscopy image of a Fe/Cr/Fe layered system patterned by an ion beam. A clear difference between the high moment and low moment areas is seen due to the observed domain patterns; (b) an AFM image of the same systems showing a tiny (the height of the step is below 3 nm) effect of the ion beam on the surface morphology of the system.

Very recently ion beam irradiation was used for patterning of the magnetic properties of Co/Pt [6, 13] and Fe/Cr [14] layered systems. The advantage of this technique is that the patterning process just slightly affects the mesoscopical and macroscopical roughness of the sample surface and its optical and tribological properties. The ion beam patterning causes atom exchange at the interfaces of the layered systems, which is the main determinant of the properties of the system. It allows one to create adjoining regions with very different magnetic properties, such as perpendicular versus in-plane magnetization in the Co/Pt systems and high moment versus low moment magnetization in the Fe/Cr systems. The effect of ion beam patterning of a Fe/Cr/Fe bilayer is demonstrated in figure 2.

## 3. Spin waves in restricted geometries and in inhomogeneous fields

Lateral patterning dramatically changes the dynamic properties of magnetic systems due to lateral confinement. Up to now two main types of confinement effect have been distinguishable: those connected with lateral wavevector quantization within a magnetic element and those connected with the inhomogeneous static internal field caused by the finite lateral size of the element. The influence of both effects on the magnetic dynamics is sometime quite complicated [8, 15]. However, in the particular case of thin elements with $d \ll w$, where $d$ is the thickness of the elements and $w$ is its lateral size, the spectrum of magnetic excitations in the element can be described on the basis of the well known properties of spin waves in magnetic films [16, 17]

The dipole-exchange spin wave spectrum in an unlimited ferromagnetic medium is given by the Herrings–Kittel formula [18]

$$\nu = \frac{\gamma}{2\pi}\left[\left(H + \frac{2A}{M_S}Q^2\right)\left(H + \frac{2A}{M_S}Q^2 + 4\pi M_S \sin^2\theta_Q\right)\right]^{1/2}, \tag{1}$$

where $\gamma$ is the gyromagnetic ratio, $A$ is the exchange stiffness constant, $\vec{H}$ and $\vec{M}_S$ are the applied magnetic field and the saturation magnetization both aligned along the $z$-axis, $\vec{Q}$ is the three-dimensional wavevector and $\theta_Q$ is the angle between the directions of the wavevector and the magnetization.

In a magnetic film with a finite thickness $d$ the spin wave spectrum is modified due to the two dimensional confinement. An approximate expression for spin wave frequencies of a film can be written in the form, analogous to equation (1) (see equation (45) in [17]),

$$\nu = \frac{\gamma}{2\pi}\left[\left(H + \frac{2A}{M_S}Q^2\right)\left(H + \frac{2A}{M_S}Q^2 + 4\pi M_S F_{pp}(qd)\right)\right]^{1/2}, \tag{2}$$

where

$$Q^2 = q_y^2 + q_z^2 + \left(\frac{p\pi}{d}\right)^2 = q^2 + \left(\frac{p\pi}{d}\right)^2. \tag{3}$$

Here in agreement with figure 1 the normal to the film surface points along the $x$-direction. $q$ is the continuously varying in-plane wavevector, $F_{pp}(qd)$ is the matrix element of the magnetic dipole interaction and $p$ is a quantization number for the so-called perpendicular standing spin waves (PSSW), which is determined by the so-called 'Rado–Wertmann' boundary conditions [19] for the dynamic part $\vec{m}$ of the magnetization on the film surfaces:

$$\pm\frac{\partial\vec{m}}{\partial x} + D\vec{m}|_{x=\pm d/2} = 0. \tag{4}$$

with the so-called pinning parameter $D$ determined by the effective surface anisotropy, $k_S$, and the exchange stiffness constant $A$: $D = k_S/A$. One can also define a pinning length $\xi = 1/D$. The physical meaning of $\xi$ is quite apparent: if the typical length of the problem (e.g., the thickness of the film, $d$) is much larger than $\xi$, a strong pinning takes place; if, in contrast, $d \ll \xi$, the mode is essentially unpinned.

If the film is magnetized in the plane and $\vec{q} \perp \vec{M}_S$, neglecting exchange ($A = 0$), the dispersion equation for the lowest thickness mode ($p = 0$) obtained from equation (2) gives results that are very similar to the results obtained by Damon and Eshbach [16]:

$$\nu_{DE} = \frac{\gamma}{2\pi}[H(H + 4\pi M_S) + (2\pi M_S)^2(1 - e^{-2qd})]^{1/2}. \tag{5}$$

In contrast, if $\vec{q}_\parallel \parallel \vec{M}_S$, the so-called backward volume magnetostatic (BVMS) mode occurs. Its dispersion is quite unusual: the wave frequency decreases with increasing wavevector.

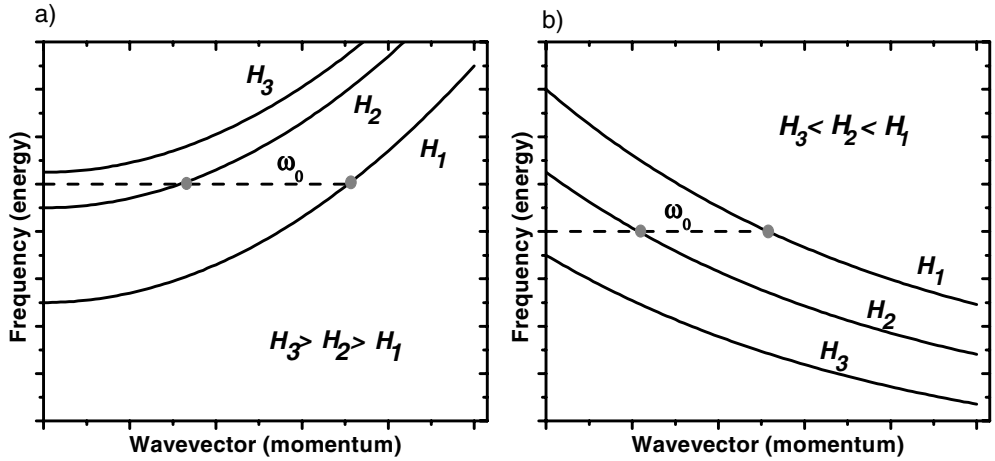


**Figure 3.** Spin wave/particle reflection by a region of inhomogeneous field/gap. (a) The wave has a positive group velocity; (b) the wave has a negative group velocity.

The above theoretical analysis is based on the Landau–Lifshitz equation [20]. Although this equation is not similar to the Schrödinger equation, describing quantum mechanical particles, properties of spin waves are very similar to those of quantum mechanical particles. The main reason for the similarity of the properties is the similarity of the dispersions of the spin waves and the particles. In fact, unlike light waves or acoustic phonons, spin waves have a gap at zero wavevector in their dispersion spectrum. The gap can be caused by different interactions: Zeeman energy of the applied field, energy of magnetic anisotropy or dipole–dipole interaction energy. For the simplest case of unconfined magnetic media and neglecting the dipole–dipole interaction and magnetic anisotropies, the spin wave dispersion spectrum can be written as follows:

$$h\nu = \hbar\omega = \Delta + \frac{2\hbar\gamma A}{M_S}q^2, \tag{6}$$

where $\Delta = \hbar\gamma H$ which is reminiscent of the dispersion of a particle in a potential field $U(x)$:

$$E = \hbar\omega_{el} = U(x) + \frac{\hbar^2}{2m}q^2. \tag{7}$$

The similarity is even more obvious if one implies that the applied field $H$ is inhomogeneous, $H(x)$:

$$h\nu = \hbar\omega = \Delta(x) + \frac{2\hbar\gamma A}{M_S}q^2. \tag{8}$$

Thus, the propagation of a spin wavepacket in an inhomogeneous magnetic field is in many of its consequences similar to that of a quantum mechanical particle: if during its propagation the packet enters a region of changing values of the gap, it must change its wavevector to fulfil the energy conservation law. If the value of the gap in some region exceeds the value of the initial energy of the magnon, the wave is reflected from the region. The effect of spin wave reflection is illustrated in figure 3. If during its propagation a wave with a frequency $\omega_0$ moves from a region with the field $H_1$ to one with the field $H_2$, there is a possibility of fulfilling the dispersion law for both $\omega_0$ and $H_2$ by decreasing the wavevector. The wave keeps propagating through the inhomogeneous field, albeit with changing wavevector. However, if the local field increases further, at some point it reaches a region with the field $H_3$, where the

minimum allowed frequency (the gap) is above $\omega_0$. There exists no real wavevector fulfilling the dispersion law for both $\omega_0$ and $H_3$. The wave must be reflected at this point. Similarly to in quantum mechanics, in addition to reflection one should expect in some cases the effect of spin wave tunnelling. The effects of spin wave reflection and tunnelling will be experimentally demonstrated in section 7 of this paper.

Note here a very peculiar feature of propagation of the BVMS wave in an inhomogeneous field. In fact, the frequency of the BVMS wave decreases with increasing wavevector and the allowed states are situated below the zero wavevector gap. Thus, to realize reflection of a spin wavepacket from the field inhomogeneity, one should not increase, but decrease the field (gap). In this sense electronic holes are the quantum mechanical counterpart of the BVMS waves. The situation is illustrated in figure 3(b).

As was discussed in the previous section lateral structuring can create confined magnetic elements with different patterns. However, in all cases the shape of the element is non-ellipsoidal. This means that the demagnetizing field (the statical as well as the dynamic one) is inhomogeneous. Together with the applied field this field produces an inhomogeneous internal field of the element. This effect is especially strong near the side edges of the element, which are perpendicular to the magnetization. For example, if a magnetic stripe is magnetized along its width a strong inhomogeneous static demagnetizing field creates regions of zero internal field near the side edges, where the static magnetization is not saturated. On the boundary between these zero field regions and the saturated regions in the middle of the stripe the field inhomogeneity reaches its maximum. Therefore, under some circumstances, a spin wave entering the saturated region from the zero field region is reflected by the field profile in the same way as was discussed above for unrestricted media. Since the wave is also confined by the stripe edges on the other side, it is localized; a so-called spin wave well is created [21, 22]. In this well, localized states are created, whose number depends on the depth of the well [23]. The spin wave well effect will be discussed in detail later in this paper.

If an element with two laterally confined dimensions is studied the internal field will be inhomogeneous at all orientations of the applied field. In contrast, if a long magnetic stripe with only one confined dimension (its width) is investigated, one can avoid any inhomogeneous static internal field, if the external field is applied along the length of the stripe. In this case the spin wave well effect is absent and the only effect of lateral confinement is spin wave quantization along the width of the stripe [24–26].

## 4. Brillouin light scattering technique

Together with FMR and time resolved magnetization measurements using magneto-optical techniques, BLS is mainly used for studies of magnetic dynamics. In the field of patterned structures BLS has a number of advantages. It combines the possibility to study the dynamics of patterned systems in the frequency range beyond 100 GHz (the corresponding time resolution is 10 ps) with a high lateral resolution of 1–2 $\mu$m defined by the size of the laser beam focus. However, as will be discussed in this section, BLS can be used in a so-called 'Fourier microscope' mode with an effective resolution below 0.2 $\mu$m. There being no need for additional excitation techniques makes BLS especially successful in studying complicated, strongly confined spin wave modes.

As illustrated in the inset of figure 4 a beam of monoenergetic photons of wavevector $\vec{q}_I$ and frequency $\omega_I = c\vec{q}_I$ interact with a magnon, described by $\vec{q}$ and $\omega$. The scattered photon gains an increase in energy and momentum:

$$\hbar\omega_S = \hbar(\omega_I + \omega) \qquad \hbar\vec{q}_S = \hbar(\vec{q}_I + \vec{q}), \tag{9}$$

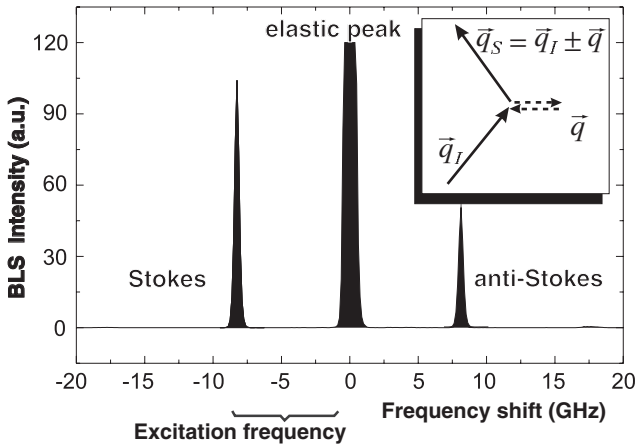


**Figure 4.** A typical spectrum of BLS from spin wave excitations. Inset: an illustration of the scattering process.

if a magnon is annihilated. From equation (9) it is evident that the wavevector $\vec{q}_S - \vec{q}_I$, transferred in the scattering process is equal to the wavevector $\vec{q}$ of the magnon. A magnon can also be created by energy and momentum transfer from the photon, which in the scattered state has the energy $\hbar(\omega_I - \omega)$ and momentum $\hbar(\vec{q}_I - \vec{q})$. Since for room temperature ($T_R \gg \hbar\omega/k_B \approx 1$ K) the two processes have about the same probability, the resulting light scattering spectrum shown schematically in figure 4 demonstrates Stokes and anti-Stokes peaks. Measuring the frequency shift of both peaks one obtains the frequency of the spin wave participating in the BLS process. Changing the scattering geometry one can sweep the value of $q$ and measure the corresponding $\omega$. Thus, the spin wave dispersion $\omega(q)$ can be studied. In a BLS experiment in opaque systems with backscattering geometry the value of the in-plane wavevector $\vec{q}$, transferred in the light scattering process, can be varied by changing the angle of light incidence, $\theta$, measured from the surface normal: $q = (4\pi/\lambda_{\text{Laser}}) \sin\theta$. The absolute value of $q$ varies in the range (0–2.5) $\times 10^5$ cm$^{-1}$ for the Ar line with its wavelength 514.5 nm. The frequency resolution of the technique is about 0.1–0.2 GHz, which corresponds to 10 mK or 1 $\mu$eV.

The differential light scattering cross section $\mathrm{d}^2\sigma/\mathrm{d}\Omega\,\mathrm{d}\omega_S$, i.e., the number of photons scattered into the solid angle $\mathrm{d}\Omega$ in the frequency interval between $\omega_S$ and $\omega_S + \mathrm{d}\omega_S$ per unit incident flux density, can be written as follows [27]:

$$\frac{\mathrm{d}^2\sigma}{\mathrm{d}\Omega\,\mathrm{d}\omega_S} \propto \langle \delta\epsilon^*(\vec{q}_I - \vec{q}_S)\delta\epsilon(\vec{q}_I - \vec{q}_S)\rangle_{\omega_I - \omega_S} \tag{10}$$

with $\delta\epsilon$ the dynamic (fluctuating) part of the dielectric permittivity, which is caused by the spin waves due to magneto-optical effects and which gives rise to the scattering. $\delta\epsilon$ is proportional to the dynamic part of the magnetization $\vec{m}$ of the spin wave. The correlation function is given by

$$\begin{aligned}
\langle \delta\epsilon^*(\vec{q})\delta\epsilon(\vec{q})\rangle_\omega &= \int \mathrm{d}(t_2 - t_1)\,\mathrm{d}^3(\vec{r}_2 - \vec{r}_1)\exp[-\mathrm{i}\omega t - \mathrm{i}\vec{q}\cdot(\vec{r}_2 - \vec{r}_1)] \\
\langle \delta\epsilon^*(\vec{r}_1, t_1)\delta\epsilon(\vec{r}_2, t_2)\rangle &\propto \int \mathrm{d}(t_2 - t_1)\,\mathrm{d}^3(\vec{r}_2 - \vec{r}_1)\exp[-\mathrm{i}\omega t - \mathrm{i}\vec{q}\cdot(\vec{r}_2 - \vec{r}_1)] \\
&\quad \times \langle \vec{m}^*(\vec{r}_1, t_1)\vec{m}(\vec{r}_2, t_2)\rangle
\end{aligned} \tag{11}$$

with $\langle\cdots\rangle$ the statistical average. For light scattered from a spin wave propagating in an infinite

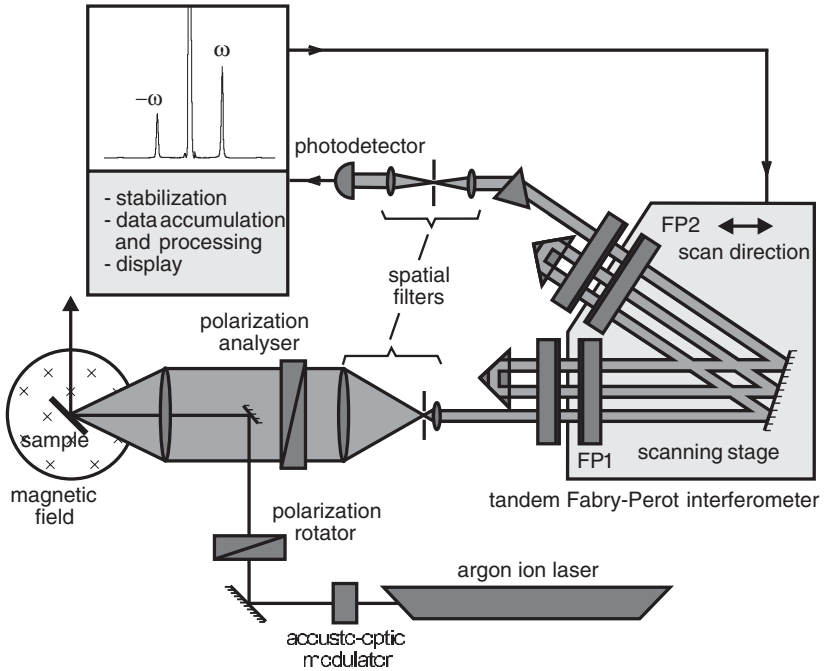


**Figure 5.** A schematic view of a BLS set-up.

medium, the spatial integration volume is the entire space. In this case the correlation function in equation (11) is nonzero only if the relations $\omega = \omega_S - \omega_I$ and $\vec{q} = \vec{q}_S - \vec{q}_I$ are fulfilled, yielding the conservation laws of energy and momentum, described by equation (9). However, if a spin wave mode propagates in a confined medium (magnetic film, stripe or dot) the integration volume is restricted by the confinement. The conservation conditions are fulfilled only for the components of the wavevector which are along the unconfined coordinates. In the case of a film these are two components of the in-plane wavevector, $\vec{q}$; in the case of a long stripe this is the component of $\vec{q}$ parallel to the stripe axis. It is also clear from equation (11) that the dependence of the differential light scattering cross section on the component of $\vec{q}$ perpendicular to the stripes is determined by the Fourier components of $\vec{m}(y)$. Below we will discuss this in more detail.

A typical experimental set-up for BLS studies is shown schematically in figure 5. Light of a frequency stabilized laser is focused onto the sample by an objective lens. The light scattered from the sample (elastic and inelastic contributions) is collected and sent through a spatial filter for suppressing background noise before entering the interferometer. The central part of the interferometer consists of two Fabry–Perot etalons FP1 and FP2. The tandem arrangement avoids ambiguities in the assignment of inelastic peaks to the corresponding transmission orders [28, 29]. In order to obtain the high contrast necessary for detecting the weak inelastic signals, the light is sent through both etalons several times using a system of retroreflectors and mirrors. The frequency selected light transmitted by the interferometer is detected by a photomultiplier or an avalanche photodiode after passing through a second spatial filter for additional background suppression. A prism or an interference filter between the second spatial filter and the detector serves for suppression of inelastic light from common transmission orders outside the frequency region of interest. Data collection is performed by a personal computer or by a multichannel analyser.

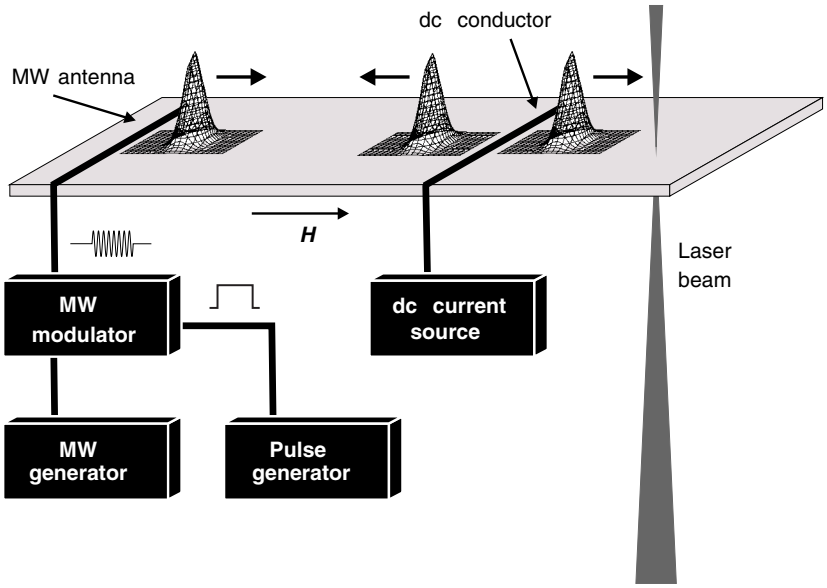


**Figure 6.** The schematic layout of the BLS set-up in the forward-scattering geometry with space and time resolution. For a discussion of the components see the main text.

## 5. Time and space resolved light scattering

An inhomogeneous internal magnetic field strongly affects dynamic properties of small magnetic elements. However, for a better understanding of dynamic properties of such elements a study of spin wave properties of magnetic systems with a macroscopical inhomogeneous applied field is very useful. As an example, an investigation of both the spatial and the temporal properties of spin wavepackets propagating in a ferrite film with an inhomogeneous applied magnetic field will be discussed in section 7. For this study a novel experimental technique—time and space resolved BLS as shown schematically in figure 6 has been used. It is based on a standard BLS set-up and was originally developed to study the propagation and interaction of nonlinear spin wavepackets in magnetic ferrite films [30]. Spin wavepackets are generated by a microwave input antenna and detected using BLS. The microwave excitation set-up needed for the excitation is built as follows. CW microwave power is created by a microwave generator. A pulse generator generates pulses of 10–30 ns duration. The pulses are sent to a microwave modulator to create a pulsed microwave field. If a microwave pulse with a frequency $\omega_0$ is applied to the input antenna, a spin wave is launched with a wavevector determined by the dispersion relation $\omega_0(\vec{q})$ of the spin wave. Spin waves are effectively excited in a wavevector interval $q < 300$ rad cm$^{-1}$, with the upper bound imposed by the width of the antenna. Since the above value is much smaller than the wavevectors of the scattering photons, the light scattered in the forward direction is investigated to achieve a high sensitivity in this low wavevector regime. The spatial distribution of the spin wavepacket is detected by scanning the laser beam across the sample; this is performed by a motorized sample mount.

Temporal resolution is added by using a time correlated single photon counting method similar to time-of-flight measurements in, e.g., mass spectroscopy. If the spin wave pulse, launched by the antenna, crosses the laser spot, light is inelastically scattered. The scattered

light passes through the interferometer and is detected by a single photon detector. The output signal from the pulse generator used in the microwave set-up also starts a system counting the elapsed delay time between the launch of the spin wave pulse and its arrival at the position of the laser spot. The output signal of the detector is used to stop the counter. The events of photon detection are then accumulated in a 16-bit memory cell of a 32 K linear memory array; the cell number is determined by the measured elapsed time. The procedure is repeated with a repetition rate of typically 1 MHz. After accumulating a large number of events the content of the memory array represents the temporal variation of the light scattering cross section (which is proportional to the spin wave intensity) at the current position of the laser spot. By repeating the procedure for different positions of the laser spot on the sample, two dimensional maps of the spin wave intensity are constructed for different values of the delay time. The data are arranged in a digital video animation with each frame representing the spatial distribution of the spin wave intensity for a given delay time. The entire system is built on the basis of a digital signal processing device which interacts with a PC via a RS232 interface. The device can handle up to $2.5 \times 10^6$ events $s^{-1}$ continuously. A lower limit of about 1–2 ns on the time resolution is imposed by the intrinsic time resolution of the BLS spectrometer. Typical accumulation times are 5 s/position of the laser spot.

Let us make a final comment on the spatial resolution of the BLS set-up. The resolution is mainly determined by the size of the laser beam focus. Due to this restriction it is impossible to determine directly the spatial profiles of spin wave modes confined in micron-size magnetic stripes and dots with a typical size of 1–2 $\mu$m. However, if BLS is used in the 'Fourier microscope' mode, the light scattering intensity is measured as a function of the transferred in-plane wavevector. As has been shown in the previous section, this intensity is proportional to the Fourier component of the spin wave mode profile. On the basis of this information the mode profile in small magnetic elements is reconstructed. In the 'Fourier microscope' mode the spatial resolution, $\delta$, is determined by the accessible transferred wavevector interval $\pi/\Delta q$. For light scattering experiments it follows $\Delta q = 2q_I$ and $\delta = 120$–$130$ nm for green laser lines. On the other hand, a typical size of the spin wavepackets used for the studies in artificially created inhomogeneous fields in ferrite films is about 0.5–1 mm. In this case the spatial profile of the packet can be measured directly, scanning the laser beam along the sample.

## 6. Effect of lateral quantization

The effect of lateral spin wave quantization within a magnetic element was discovered several years ago using BLS [24] and is described in detail in original papers [25] and reviews [26, 31]. Here we will just present the most important features of the effect. In its clearest form it takes place if, e.g. a long magnetic stripe is magnetized along its length. In this case the static internal field is homogeneous within the stripe and equal to the static external field, $H_i = H_e$. The side boundary of the stripe causes the quantization of the spin wave wavevector, which manifests itself in quantized frequencies of the modes and gaps in the spin wave dispersion spectrum. Figure 7 demonstrates the experimentally measured spin wave dispersion in an array of magnetic stripes with a thickness of $d = 40$ nm, a width of $w = 1.8$ $\mu$m and with different separations (0.7 and 2.2 $\mu$m).

Clear modification of spin wave dispersion with creation of spin wave modes with quantized frequencies and gaps in the dispersion is seen. From the fact that there is no noticeable difference between the data for the samples with the same stripe width but different stripe separations one can conclude that a single stripe effect is observed. The observed quantized modes can be understood as Damon–Eshbach-like modes with a quantized wavevector parallel

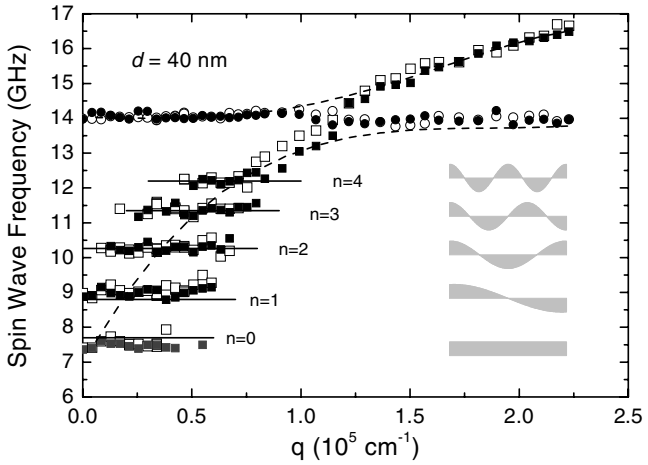


**Figure 7.** The spin wave dispersion curves obtained for an array of stripes of thickness 40 nm, width 1.8 $\mu$m and separations between stripes of 0.7 $\mu$m (open symbols) and 2.2 $\mu$m (solid symbols). The external field applied along the stripe length is 500 Oe. The horizontal lines indicate the results of a calculation based on the approach described, with the quantized values of $q$ obtained for the unpinned boundary conditions. The dashed lines showing the hybridized dispersion of the Damon–Eshbach mode and the first PSSW mode were calculated numerically for a continuous film with a thickness of 40 nm. On the right-hand side the mode profiles are illustrated. The samples were prepared using XRL.

to the stripe width. For the calculation of the quantized values of the wavevector and, thus, mode frequencies, a boundary condition on the side edges of the stripe ($y = \pm w/2$) similar to equation (4) has been proposed in [24, 25]. The pinning length, $\xi$, was set to be infinite, corresponding to the pinning parameter $D = 0$, which is justified by the small values of anisotropies in permalloy. As is seen in figure 7 the approach nicely describes the experimental data presented. The same approach was used for calculation of the mode profiles, also shown in the figure. However, the data obtained later for samples with smoother side edges prepared using EBL cannot be described using unpinned boundary conditions. Very recently a thorough theoretical analysis of the problem [32] has shown that the inhomogeneity of the dynamic internal field near the side edges of the stripe causes a 'dipolar pinning' which has, mathematically, the same form as the Rado–Wertmann exchange boundary conditions:

$$\pm\frac{\partial\vec{m}}{\partial y}+\frac{1}{\xi}\vec{m}|_{y=\pm w/2}=0. \tag{12}$$

The pinning length in this case is determined as follows:

$$\xi\approx d\frac{1+2\ln(w/d)}{2\pi}. \tag{13}$$

From equation (13) it is clear that in thin stripes ($w \gg d$) a strong pinning should be observed for low index modes. It is, however, necessary to make three important remarks in connection with equations (12) and (13):

(i) For a particular quantized spin wave mode the pinning scale $\xi$ slightly depends on the mode number, i.e., the mode profile.
(ii) Even at constant $\xi$, the pinning strength, which is determined as the ratio of the mean value of the dynamic magnetization $\int m_n(y)\,\mathrm{d}y/w$ to its value at the edges $m_n(y)_{y=w/2}$, decreases with the mode number, $n$, since the typical length determined by $m_n(y)$ scales

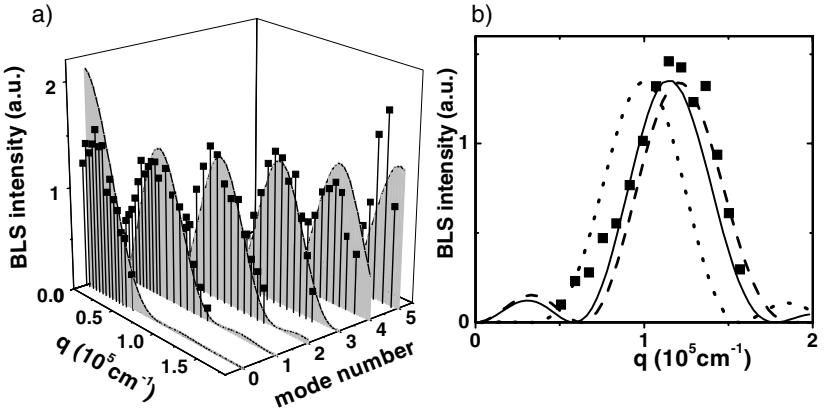


**Figure 8.** (a) Measured BLS intensities (black squares) of an array of stripes (thickness 33 nm, width 1 $\mu$m, separation 0.3 $\mu$m) as a function of the wavevector $q$ and the mode number $n$. The grey profiles illustrate the results of calculation based on the approach of lateral spin wave quantization with the dipole pinning. (b) Detailed data for the quantized mode with $n = 3$. Solid curve: the same as in (a); dashed curve: complete pinning; dotted curve: unpinned mode.

with $n$ as $\sim w/n$. Thus, the typical length approaches the pinning length, $\xi$ and, as was discussed in section 3, the pinning is not so strong.

(iii) The above approach is only applicable if the side edges are smooth, the smoothness scale being determined not by the width of the stripe, but by its thickness. In fact, the strong inhomogeneous dynamic dipole field responsible for the dipole pinning is mainly concentrated near the edges within a distance comparable with the thickness of the stripe. If the edges are rough on that scale, the dipole field is strongly affected by the roughness.

The success of the above approach is demonstrated by figure 8, showing the experimentally measured BLS intensity of different modes in an array of magnetic stripes with a thickness of $d = 33$ nm, a width of $w = 1.0$ $\mu$m and a separation of 0.3 $\mu$m, prepared using EBL, together with the theoretical profiles calculated on the basis of the approach of quantized spin wave modes with the effective dipole pinning on the side edges. The agreement between the experimental data and the result of the calculation is remarkable. To emphasize the importance of the boundary conditions the data for the quantized mode with $n = 3$ are compared with several theoretical curves: the solid curve was calculated using the correct dipole pinning, the dashed curve corresponds to complete pinning and the dotted curve represents the unpinned mode. The figure clearly demonstrates the ability of the BLS method in the Fourier microscope mode to provide detailed information on profiles of the quantized modes.

## 7. Propagation, reflection and tunnelling of spin waves

The physical origin of the spin wave quantization effects is the lateral confinement due to lateral edges of the element. This effect has not very much to do with inhomogeneity of the internal field in the element; it has been discovered in magnetic stripes with a homogeneous internal field. However, as will be discussed in the following section, a strongly inhomogeneous internal field in the element resulting from demagnetizing effects can cause turning points within the element which reflect spin waves and thus create a spin wave well.

One can model and visualize turning points for spin waves experimentally in an unconfined magnetic film, applying an inhomogeneous external field. For these experiments the space and

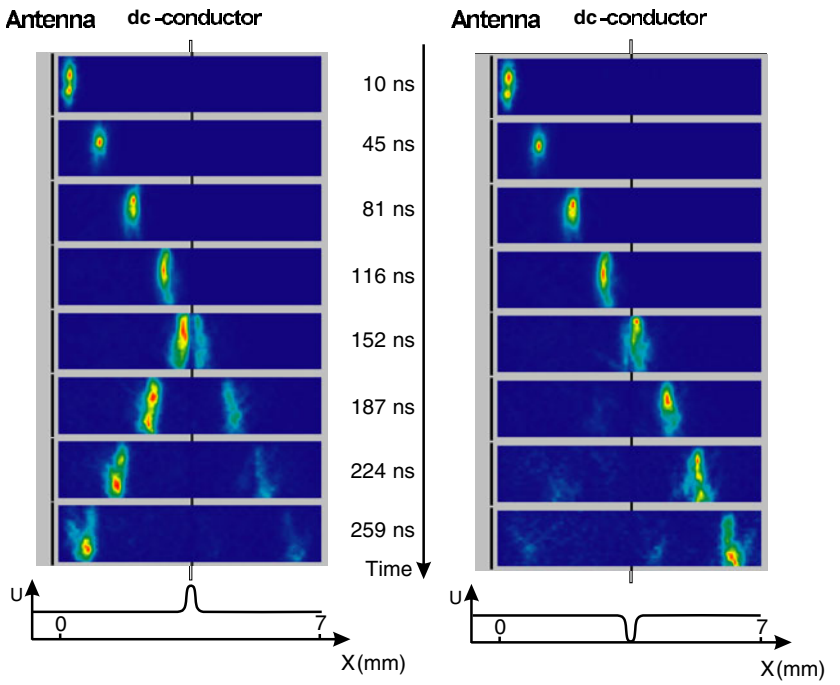


**Figure 9.** Propagation of a BVMS spin wavepacket across a YIG film with local field inhomogeneity, observed by means of space and time resolved BLS. Snapshots of the two dimensional spin wave intensity at given delay times indicated in the middle are shown. The left panel represents the case of a local maximum of the field, corresponding to a potential dip; the right panel represents the case of a local minimum of the field, corresponding to a potential well. The field profiles are displayed in the bottom graphs.

time resolved BLS technique discussed in section 5 is very useful (see figure 6). Spin wavepackets in a transparent yttrium iron garnet (YIG) film are generated by a microwave input antenna and are detected using BLS. In addition to the described components of the technique a narrow conductor of 50 $\mu$m diameter mounted across the film carrying a dc current is used to create an inhomogeneous field.

The antenna is connected to a pulsed microwave source with carrying frequency $\omega_0/2\pi =$ 7.315 GHz. An external field is oriented parallel to the film and the propagation direction of the spin waves. As is discussed above, such a set-up corresponds to the BVMS wave geometry, characterized by a negative group velocity of the spin waves [26]. For the value used for the external field $H_e = 1898$ Oe BVMS waves with a wavevector of 120–130 cm$^{-1}$ are excited. The maximum inhomogeneous field created by the dc conductor is about 20 Oe, a value which is much smaller than $H_e$. Nevertheless, such a small field can strongly disturb the spin wave propagation.

Spin waves in an inhomogeneous field have already been discussed in section 3. Depending on the direction of the dc current, the total field (and, thus, the gap of the spin wave spectrum) is locally either enhanced or reduced by the Oersted field generated by the current flowing through the conductor. If the inhomogeneity is strong enough and has an appropriate sign it serves as a turning point for the spin wave and reflects the spin wavepacket. Such a reflection is experimentally demonstrated in figure 9. Shown are two sequences of snapshot frames for different delay times as indicated. The images put in the left panel are measured for an enhancement of the local field by the dc current, whereas the right panel corresponds to a

reduced local field. Each snapshot displays the normalized two dimensional distribution of the spin wave intensity over the film, presented via a colour code.

The left panel of figure 9 demonstrates spin wave propagation in the film. As is discussed above, a region of slightly enhanced local field cannot be a turning point for a BVMS wavepacket. The wave accommodates its wavevector according to the dispersion law and passes the region of field inhomogeneity. The weak reflection observed in the frames is due to the non-adiabatical nature of the process: in fact the wavelength of the wave in not much smaller than the width of the region.

Much more interesting effects are presented in the right panel corresponding to a reduced local field. One can easily see that the region of a reduced field inhibits propagation of spin waves. If due to field reduction the maximum value of the BVMS wave frequency (the gap in the dispersion) is below the spin wave frequency of the packet, the region of the field reduction serves as a turning point for the packet and reflects it. In fact, it is a forbidden region for the wave, since there exist no BVMS waves with real wavevectors in the region. This effect is reminiscent of the quasi-classical quantum mechanical problem of particle reflection and tunnelling. Indeed, the right panel of figure 9 demonstrates that the spin wavepacket is partially reflected and partially transmitted by the forbidden region. Despite the obvious similarity with the quantum mechanics problem, the physics of the spin wave tunnelling has not become clear so far. In contrast to the case of the Schrödinger equation having wavefunction solutions with imaginary wavevectors for the 'forbidden' energies, the exact solution of the Landau–Lifshitz equation with an inhomogeneous applied field for imaginary wavevectors is not obvious, since a long range magnetic dipole interaction must be taken into account.

## 8. Spin wave wells

In this section we discuss dynamic excitations in small magnetic items (long stripes and rectangular elements) with a large inhomogeneity of the internal field. It is known that in a non-ellipsoidal element the internal field decreases near the edges of the element [33]. In some cases zones with zero internal fields can be created [34]. The problem of inhomogeneous internal field has been avoided in section 6, where the spin wave quantization in stripes has been discussed, since the external field was applied along the long axis of the stripes.

In the following discussion we assume a Cartesian coordinate system, as shown in figure 1, in which the $x$-axis is perpendicular to the plane of the elements and the $y$-axis is along the long axes of the stripes. The wavevector $\vec{q}$ is chosen along the $z$-axis, i.e., perpendicular to the stripes. Figure 10 shows two typical BLS spectra obtained from an array of stripes of a width $w = 1$ $\mu$m, a length of 90 $\mu$m and a distance between the stripes of 0.5 $\mu$m for the external in-plane magnetic field $H_e = 500$ Oe for different orientations of the field. A spectrum for an unstructured film of the same thickness is also shown for comparison. Spectrum (a) is obtained for $\vec{H}_e$ oriented along the $y$-axis, thus representing the DE geometry, discussed above. Spectrum (b) is recorded with both $\vec{q}$ and $\vec{H}_e$ aligned along the $z$-axis. As is seen in figure 10 both spectra contain several distinct peaks corresponding to spin wave modes. The high frequency peaks indicated as PSSW can be easily identified as exchange dominated PSSW modes also observed in unpatterned films. Their frequencies are determined by the exchange interaction and the internal field.

To investigate the nature of the other observed excitations, the dispersion was measured by varying $q$. It is displayed in figure 11 for both orientations of $\vec{H}_e$.

Figure 11(a) representing the DE geometry clearly demonstrates the lateral quantization of the DE spin waves, resembling a typical 'staircase' dispersion, discussed in section 1.5. The interval of the observation of each mode in the $q$-space $\Delta q \approx (0.8\text{–}1.0) \times 10^5$ cm$^{-1}$

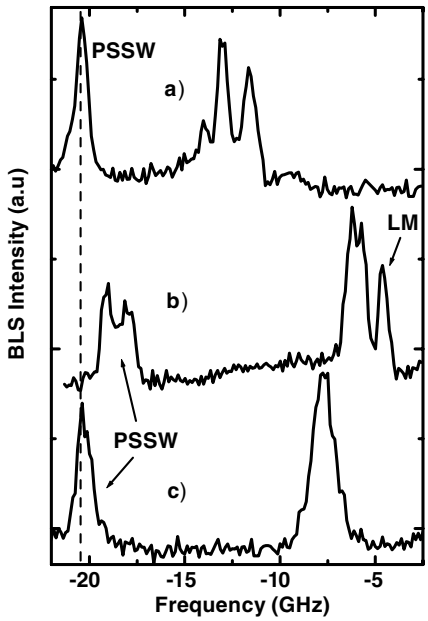


**Figure 10.** BLS spectra obtained for the stripe array for $q = 1 \times 10^5$ cm$^{-1}$ at $H_e = 500$ Oe. Spectra (a) and (b) correspond to different experimental geometries as described in the text, while spectrum (c) is obtained for an unstructured film. PSSW stands for perpendicular standing spin wave; LM stands for localized mode.

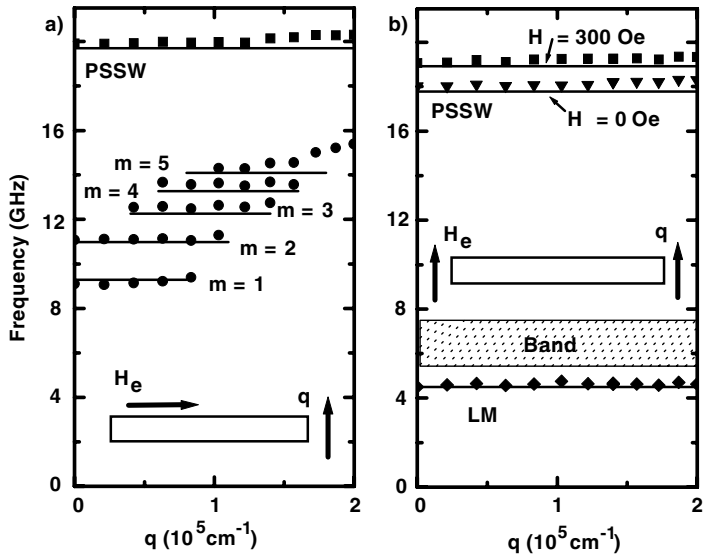


**Figure 11.** Spin wave dispersion of the stripe array measured at $H_e = 500$ Oe for (a) the DE geometry, (b) the BVMS geometry. The solid lines represent the results of calculation.

is in agreement with the width of the stripe $w = 1$ $\mu$m, giving $2\pi/w = 0.63 \times 10^5$ cm$^{-1}$. The frequency of the PSSW mode coincides with that of the PSSW mode for the unpatterned

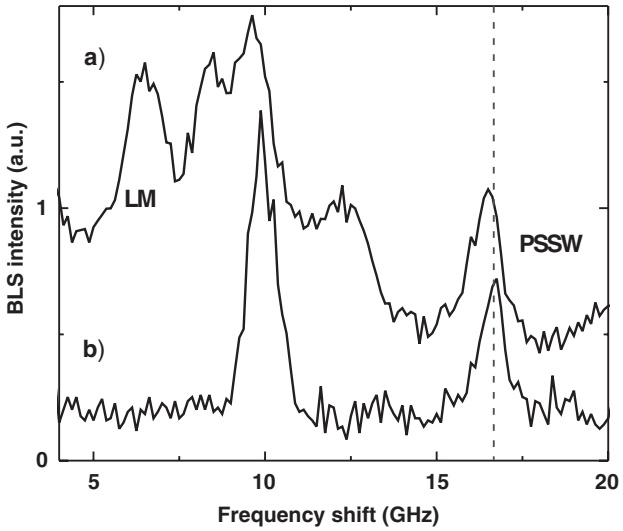


**Figure 12.** (a) The BLS spectrum obtained at $H_e = 600$ Oe for the array of rectangular elements with lateral sizes $1 \times 1.2\ \mu m^2$, distance between the elements $\delta = 0.3\ \mu$m and thickness $d = 35$ nm for $q = 0.4 \times 10^5\ cm^{-1}$. The field is applied along the long axis of the element. (b) The BLS spectrum of a continuous film for the same values of the field and the wavevector.

film and corresponds to an internal field of $H = H_e = 500$ Oe, thus corroborating negligible demagnetizing effects in the stripes magnetized along their long axes.

The dispersion presented in figure 11(b) for $\vec{H}_e$ parallel to the $z$-axis (i.e. $\vec{H}_e \parallel \vec{q}$, the BVMS geometry) differs completely from that shown in figure 11(a). First, the PSSW mode is split into two modes, with frequencies corresponding to internal fields of $H = 300$ and 0 Oe, respectively. This corroborates the well known assertion that the internal field is determined by essential demagnetizing effects and can be zero near the stripe edges [34]. Second, a broad peak is seen in the spectra in the frequency range 5.5–7.5 GHz over the entire accessible interval of $q$. The shape of the peak varies with $q$, thus indicating different contributions of unresolved laterally quantized modes to the scattering cross section at different $q$. Third, a separate, low frequency, dispersionless mode with a frequency near 4.6 GHz (indicated as 'LM' in figures 10 and 11) is observed over the entire accessible wavevector range ($q_{lim} = 2.5 \times 10^5\ cm^{-1}$) with almost constant intensity. This is a direct confirmation of a strong lateral localization of the mode within a region with the width $\Delta r < 2\pi/q_{lim} = 0.25\ \mu$m. From the low frequency of the mode one can conclude that it is localized near the edges of the elements, since these are the field-free regions [33, 34].

Further evidence for the existence of localized modes in structured systems is provided by the observation of a corresponding mode in rectangular elements. For example, figure 12 demonstrates a BLS spectrum taken for an array of rectangular elements with lateral sizes $1 \times 1.2\ \mu m^2$, distance between the elements $\delta = 0.3\ \mu$m and thickness $d = 35$ nm. The peak near 6.5 GHz is clearly identified as a localized mode due to its observation over the entire range of accessible wavevectors. Similarly to the case for the stripes a frequency shift of the PSSW mode with respect to that of a continuous film is seen in figure 12. However, one should mention here that the identification of the modes observed in rectangular elements is more complicated than for the case of the stripes. This is connected with a more complicated, two dimensional mode quantization in the elements.

A quantitative analytical description of the spin wave modes observed in the stripes is as follows. As is discussed in section 3 the frequency of the spin wave, $\nu$, depends on the angle between the in-plane wavevector and the static magnetization. The former can be written as $\vec{q} = q_y\vec{e}_y + q_z\vec{z}$. If, for reference, $\vec{H}_e \parallel \vec{e}_y$ and $\vec{q} \parallel \vec{e}_z$ (DE geometry), the analysis of spin wave quantization is straightforward [25]. One assumes a quantization condition for $q$: $q = m\pi/w$ where $m = 1, 2, 3, \ldots$. The frequencies of these quantized modes calculated using equation (2) for $m = 1, 2, 3, 4, 5$ (laterally quantized modes) and for the PSSW mode are in good quantitative agreement with the results of the experiments as shown in figure 11(a). The material parameters used are: $4\pi M_S = 10.2$ kOe, $A = 10^{-6}$ erg cm$^{-2}$, $\gamma/2\pi = 2.95$ GHz kOe$^{-1}$.

If $\vec{H}_e \parallel \vec{e}_z$, the effect of demagnetization due to the finite stripe width is very large and the internal magnetic field is strongly inhomogeneous and differs from $H_e$. It can be evaluated as [33, 34]:

$$H(x, y, z) = H_e - N_{zz}(x, y, z) \times 4\pi M_S \tag{14}$$

where $N_{zz}(x, y, z)$ is the demagnetizing factor. This inhomogeneous field creates a potential well for spin waves resulting in localization. The averaged value of $H(z)$ obtained by integrating equation (14) along the axes $x$ and $y$ over the stripe cross section is shown in figure 14. For $H > 0$ the magnetization is parallel to $\vec{H}_e$. Near the edges, however, regions with $H = 0$ and with continuously rotating magnetization are formed [34]. Since the rotation of the static magnetization dramatically changes the dispersion of spin waves [16], regions with zero internal field reflect spin waves propagating from the middle of the stripe towards these regions. On the other hand, a spin wave propagating in an inhomogeneous field might encounter the second turning point even if the magnetization is uniform. As is discussed above, for large enough values of the internal field there are no allowed real values of $q$ consistent with the spin wave dispersion [35]. Thus, a potential well for propagating spin waves is created. Similarly to the case for the potential well in quantum mechanics, the conditions determining the frequencies $\nu_n$ of possible spin wave states in the well created by the inhomogeneous internal field are determined by the equation

$$2\int q[H(z), \nu]\,\mathrm{d}z = 2r\pi, \tag{15}$$

where $r = 1, 2, 3, \ldots$ and $q[H(z), \nu]$ is found from the spin wave dispersion. This states that the total phase shift of a wave propagating from one turning point to another and then returning is a multiple of $2\pi$. As will be discussed below, additional phase jumps can appear at the turning points. These jumps are firstly neglected in our analysis for the sake of clarity.

We will illustrate these ideas in the following. The dispersion curves for spin waves with $\vec{q} \parallel \vec{H}$ and $p = 0$ calculated using equation (2) for different constant values of the field are presented in figure 13. A dashed horizontal line shows the frequency of the lowest spin wave mode $\nu_1 = 4.5$ GHz obtained from equation (15) for $r = 1$ in good agreement with the experiment. It can be seen from figure 13, that for $H > 237$ Oe there are no spin waves with the frequency $\nu_1 = 4.5$ GHz. Therefore, the lowest mode can only exist in the spatial regions in the magnetic stripe where 0 Oe $< H <$ 237 Oe. The corresponding turning points are indicated in figure 14 by the vertical dashed lines. Thus, the lowest mode is localized in the narrow region $\Delta z$ near the lateral edges of the stripe where $0.26 < |z/w| < 0.39$. The mode is composed of exchange dominated plane waves with $q_{min} < q < q_{max}$, as indicated in figure 14.

The higher order spin wave modes with $r > 1$ having their frequencies above 5.3 GHz are not strongly localized and exist anywhere in the stripe where the internal field is positive

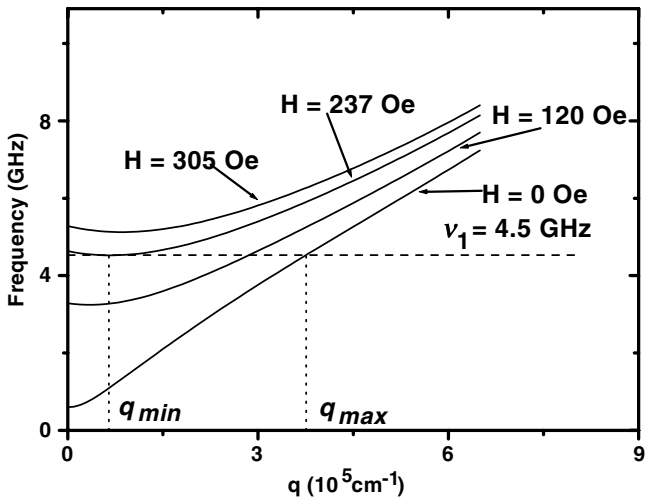


**Figure 13.** Dispersion of plane spin waves in the BVMS geometry at constant internal fields as indicated.

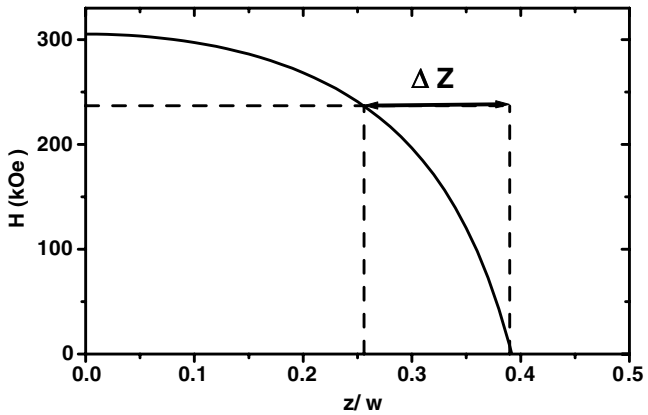


**Figure 14.** The profile of the internal field in a stripe. $\Delta z$ shows the region of the lowest mode localization.

$(0 < |z/w| < 0.39)$. In the experiment they show a band, since the frequency difference between the $\nu_r$- and $\nu_{r+1}$-modes is below the frequency resolution of the BLS technique.

The above presented one dimensional analytical approach is applicable to long magnetic stripes. To describe the spin wave modes of two dimensional rectangular magnetic elements micromagnetic simulations of nonuniform magnetic excitations in such elements have been performed [36]. The method used is based on the Langevin dynamics; the time evolution of the magnetization distribution in the magnetic element, which is discretized into $N_x \times N_z = 100 \times 180$ cells with magnetic moments $\vec{\mu}_i$, is simulated using the stochastic Landau–Lifshitz–Gilbert (LLG) equation [36]. The effective field $\vec{H}_i^{\text{eff}}$ acting on the $i$th moment consists of a deterministic part $\vec{H}_i^{\text{det}}$ (which includes an external magnetic field and the fields created by the exchange and dipolar interactions between different cell moments) and a fluctuating part $\vec{H}_i^{\text{fl}}(t)$. The correlation properties of this fluctuating field, which is intended to simulate the influence of thermal fluctuations, may be quite complicated in a micromagnetic system with

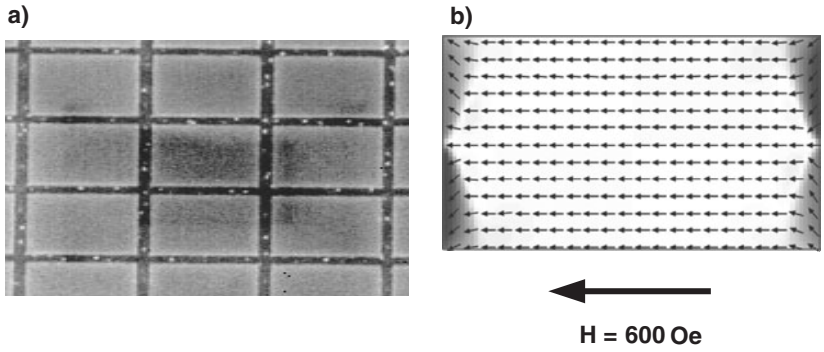


**Figure 15.** (a) An AFM image of rectangular elements; (b) the calculated distribution of static magnetization in an element.

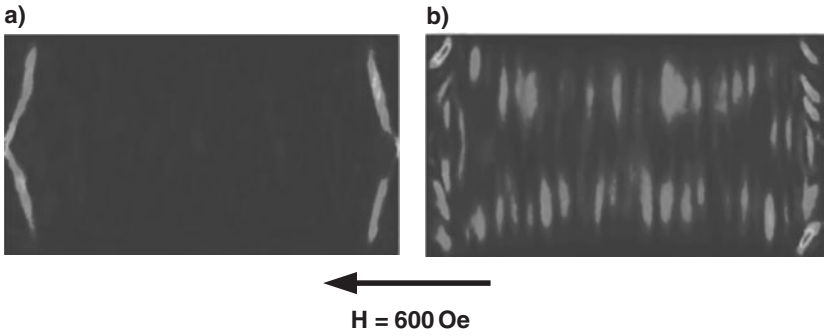


**Figure 16.** (a) A mode profile of a low frequency spin wave mode with $\nu = 5.3$ GHz (note the mode localization near the edges) in the rectangular elements; (b) a mode profile of a spin wave mode with $\nu = 12.2$ GHz.

interaction in contrast to the standard single particle situation [37]. These properties have not been studied so far. It is, however, common practice to use a simple approximation describing the fluctuating field in the form of $\delta$ correlated random noise [36, 38, 39]. We believe that the results of simulations with such a delta correlated noise should provide at least qualitatively a correct picture of the spatial distribution of different magnetic eigen-modes in the system. In the framework of this approximation the noise power has been calculated for a system of interacting magnetic cells as in [38]. The stochastic LLG equation was then solved using the modified Bulirsch–Stoer method.

The results of the simulation are presented in figures 15 and 16. Figure 15(a) presents a scanning force microscope image of the rectangular elements studied. Figure 15(b) shows the distribution of the static magnetization obtained by solving the LLG equation without any fluctuations and used as a starting point for the dynamic simulation. Next the field $\vec{H}_i^{\mathrm{fl}}(t)$ was turned on. After the thermodynamic equilibrium state of the system was reached, the values obtained for all cell moments were recorded. Afterwards, using Fourier analysis, the oscillation spectrum of the total magnetic moment of the element was obtained. In the frequency interval 3–20 GHz this Fourier spectrum demonstrates several maxima. The Fourier components of each cell magnetization $\boldsymbol{\mu}_{i,\omega}$ corresponding to these maxima were calculated and squared, to allow comparison with the measured spin wave intensities. As an example, the spatial distributions obtained for the frequencies $\nu = 5.3$ and 12.2 GHz are presented

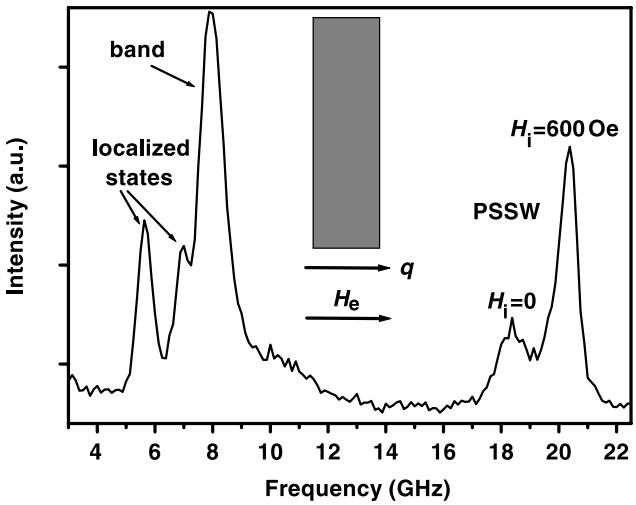


**Figure 17.** The BLS spectrum for a transferred wavevector $q = 0.47 \times 10^5$ cm$^{-1}$ and an external field of $H_e = 800$ Oe. The inset shows the experimental geometry used.

in figures 16(a) and (b). It is clear from figure 16(a) that the low frequency mode is strongly localized in the narrow regions near the edges of the elements that are perpendicular to the applied field. In contrast, and for comparison, the mode with $\nu = 12.2$ GHz shown in figure 16(b) is not localized.

Thus, we have shown that a strong inhomogeneity of the internal field causes the creation of 'spin wave wells' (SWW) in magnetic stripes and rectangular elements and the localization of spin wave modes in these wells. It is clear from the above consideration that the number of states localized in the well depends on the depths of the well, which is controlled by the value of the applied external field. This is demonstrated in figure 17. Shown is a BLS spectrum for a transferred wavevector $q = 0.47 \times 10^5$ cm$^{-1}$ for a higher external field of $H_e = 800$ Oe instead of 500 Oe as is the case for figure 10. As is seen, in addition to the PSSW modes the spectrum contains two spin wave eigenstates of the SWW (instead of one as in figure 10).

Figure 18 shows the dependence of the frequencies of the observed modes on $H_e$. While the magnitude of $H_e$ is small and not sufficient to saturate the stripe, only a single PSSW mode corresponding to $H_i = 0$ is present in the spectrum. At some critical field $H_e = H^*$ the PSSW peak begins to split. The first peak corresponding to $H_i = 0$ retains its frequency, but loses its intensity with increasing $H_e$. The frequency of the second peak (which appears at $H_e = H^*$) increases with the applied field, indicating the increase of $H_i$ in the central part of the stripe. The observed value of the critical field $H^* = 220$ Oe is in agreement with the calculated demagnetizing field in the stripe centre, $H_d(y = 0)$, based on the approach presented in [33]. Static magnetometry also shows a sharp increase of the stripe magnetic moment for $H_e > H^*$, indicating partial magnetic saturation of the stripe.

For $H_e > H^*$ a broad band of non-resolved spin wave excitations is seen [21] in the low frequency part of experimental spectra. At higher $H_e$ at first one and then more narrow peaks are observed in addition to the band. To understand the appearance of several multiple states in a SWW, one should take into account that the depth of the well strongly depends on $H_e$. In fact, the bottom of the well corresponds to $H_i = 0$ independently of $H_e$. The field which determines the position of the top of the well, however, can be roughly estimated as $H_e - H_d(y = 0) \approx H_e - H^*$. For a small difference $H_e - H^*$ the well is too shallow and there is

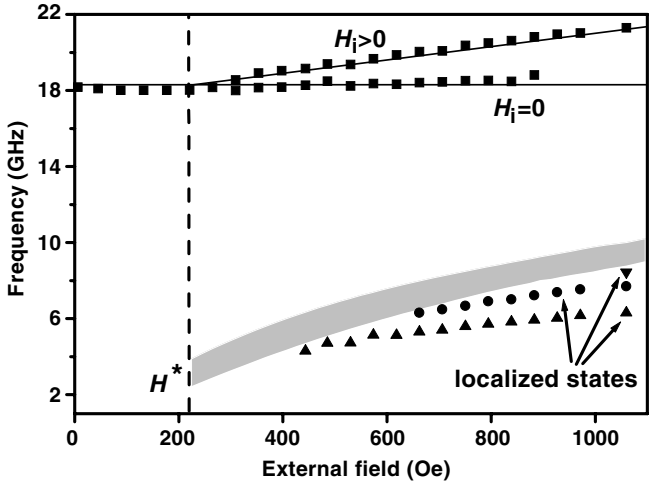


**Figure 18.** Frequencies of the modes observed in the stripes at $q = 0.47 \times 10^5$ cm$^{-1}$ as a function of $H_e$. The vertical dashed line marks the critical field $H^*$. Note the constant frequency of one PSSW mode and the increase in frequency for the other mode for $H_e > H^*$. The grey region illustrates the band of non-resolved laterally quantized excitations.

no room in the well for a localized spin wave state. With increasing $H_e$ the well becomes deeper and, as a result of that, at first one and then more localized spin wave states appear in the well.

To obtain a complete quantization condition for localized spin wave states in a SWW, we need to modify equation (15) by adding phase jumps at the turning points of the SWW:

$$\Delta\phi_l + \Delta\phi_r + 2 \times \int_{y_l}^{y_r} q(H_i(y), \nu)\, dy = 2n\pi, \tag{16}$$

where $n = 1, 2, 3, \ldots$ and $\Delta\phi_l$, $\Delta\phi_r \in [0, \pi]$ are the phase jumps at the left and right turning points, respectively. Henceforth we will call the third term in (16) the quantization integral. Note that since the dispersion of a spin wave differs from that of an electron, the results for the phase jumps obtained for an electron in a quantum well may not be used for SWW. However, the difference between the quantization integrals calculated for two successive modes should be equal to $2\pi$, if $\Delta\phi_l$ and $\Delta\phi_r$ are the same for all the localized modes.

To determine the turning points and the quantization integrals for the different spin wave states in the SWW, the profile of $H_i$ in the saturated region (see the solid curve in figure 19) has been calculated using the approach proposed in [33]. The equation $\nu = \nu(q(y), H_i(y))$ has been numerically solved for the experimentally measured values of $\nu$. As is discussed above, the point at which the solution $q(y)$ does not exist for real $q(y)$ is the turning point. The second turning point was assumed to be at the boundary between the saturated and zero field regions. Based on the obtained dependences $q(y)$ the quantization integrals for the modes have been calculated.

The main results of the calculation can be summarized as follows:

(a) The calculated quantization integrals for the localized states in the SWW decrease with increasing external field, probably due to the field dependence of $\Delta\phi_l$, $\Delta\phi_r$.
(b) The localization length $\xi = y_r - y_l$ is about 50 nm for the lowest localized state and 200–300 nm for the states having higher frequency. The localization lengths decrease with increasing $H_e$.

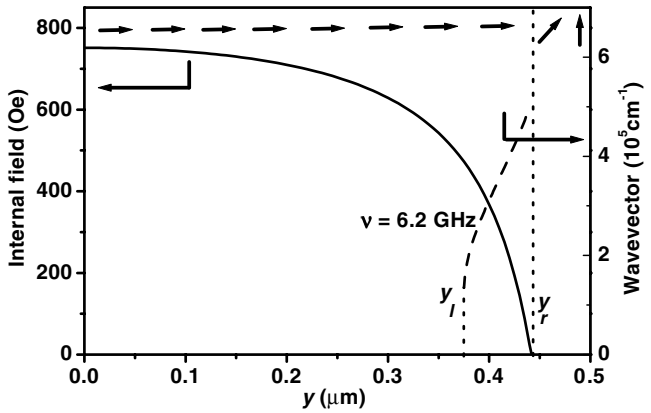


**Figure 19.** The internal field (solid curve) and wavevector of the observed states (dashed lines) calculated as functions of $y$ for an applied field of 970 Oe. $y_l$ and $y_r$ are the turning points of the localized modes with the frequencies as indicated. The arrows at the top of the figure illustrate the orientation of the static magnetization.

(c) Although the quantization integrals for two lowest localized modes depend on $H_e$, their difference is almost constant and equal to $(4.2 \pm 0.4)\pi$. This is a direct confirmation of the applicability of the quasi-classical quantization conditions (15) and (16) to the spin wave modes localized in a SWW.

The fact that the difference between the quantization integrals corresponding to the two lowest localized spin wave states in the SWW is close to $4\pi$ (and not to $2\pi$) suggests that only the two odd-numbered modes ($n = 1$ and 3) are detected having a similar (symmetrical) distribution of the spin wave intensity about the centre of the well. The reason that only the symmetric modes in the BLS experiment are seen is related to the strong spatial localization of these modes: $q\xi \ll 1$, where $q = (1\text{–}2) \times 10^5$ cm$^{-1}$ is a typical wavevector transferred in the BLS process. This inequality means that the light fields are practically homogeneous on the spatial scale of the spin wave mode localization length and, similarly to the case for standing spin wave resonance experiments [40], only the odd (symmetric) spin wave states contribute to the observed BLS intensity [25].

## 9. Conclusions

In this paper we have discussed the dynamic eigen-modes of confined magnetic objects. These modes have inherited some properties of plane spin waves, which are dynamic eigen-modes of unrestricted magnetic media. However, effects caused by confinement result in new features distinguishing the spin wave modes in confined elements from the spin waves. We mention here a discrete dispersion spectrum of the modes due to lateral quantization. It is found that an inhomogeneous internal field present in all practically important objects strongly affects their magnetic dynamics. The phenomenon of mode localization of the mode in a small part of the object due to the inhomogeneous internal field has been discussed in detail.

Studies of magnetic dynamics in inhomogeneous fields have opened a new approach to fundamentals of dynamic magnetic eigen-modes. It is now clear that they can be described in a similar way to electrons and holes in solid state physics. For example, spin wave reflection and tunnelling through a magnetic barrier are experimentally observed. This new field is currently expanding and a deep understanding still needs to be achieved. In general, the magnetic

dynamics of confined objects is an exciting field with probably many new discoveries and potential applications to come.

## Acknowledgments

The author is indebted to B Hillebrands for his continuous support, to C Chappert, C Fermon, A Slavin and D Berkov for a close collaboration and many stimulating discussions and to C Mathieu, J Jorzick, O Serha, C Bayer and V Demidov for their contributions. Financial support from the Deutsche Forschungsgemeinschaft through the Priority Programme 1133 'Ultrafast Magnetization Processes' and from the NSF is gratefully acknowledged.

## References

[1] Bloch F 1930 *Z. Phys.* **61** 206
[2] Griffiths J H E 1946 *Nature* **158** 670
[3] Fleury P A, Parto S P C, Cheesman L E and Guggenheim H J 1966 *Phys. Rev. Lett.* **17** 84
[4] Awschalom D D and DiVincenzo D P 1995 *Phys. Today* **48** 43
[5] Hehn M, Ounadjela K, Bucher J P, Rousseaux F, Decanini D, Bartenlian B and Chappert C 1996 *Science* **272** 1782
[6] Chappert C, Bernas H, Ferre J, Kottler V, Jamet J-P, Chen Y, Cambril E, Devolder T, Rousseaux F, Mathet V and Launois H 1998 *Science* **280** 1919
[7] Wernsdorfer W, Hasselbach K, Mailly D, Barbara B, Benoit A, Thomas L and Suran G 1995 *J. Magn. Magn. Mater.* **145** 33
[8] Cowburn R P 2000 *J. Phys. D: Appl. Phys.* **33** R1
[9] Kraus P R and Chou S Y 1995 *J. Vac. Sci. Technol.* B **13** 2850
[10] New M H, Pease R F W and White R L 1995 *J. Vac. Sci. Technol.* B **13** 1089
[11] Barr R O, Yamomoto S Y and Schultz S 1997 *J. Appl. Phys.* **81** 4730
[12] Rousseaux F, Decanini D, Carcenac F, Cambril E, Ravet M F, Chappert C, Bardou N, Bartenlian B and Veillet P 1995 *J. Vac. Sci. Technol.* B **13** 2787
[13] Devolder T, Chappert C, Chen Y, Cambril E, Bernas H, Jamet J-P and Ferre J 1999 *Appl. Phys. Lett.* **74** 3383
[14] Demokritov S O, Bayer C, Rickart M, Poppe S, Fassbender J, Hillebrands B, Kholin D I, Kreines N M and Liedke O M 2003 *Phys. Rev. Lett.* **90** 097201
[15] Mathieu C, Hartmann C, Bauer M, Büttner O, Riedling S, Roos B, Demokritov S O, Hillebrands B, Bartenlian B, Chappert C, Rousseaux F, Decanini D, Cambril E, Müller A, Hoffmann B and Hartmann U 1997 *Appl. Phys. Lett.* **70** 2912
[16] Damon R W and Eshbach J R 1961 *J. Phys. Chem. Solids* **19** 308
[17] Kalinikos B A and Slavin A N 1986 *J. Phys. C: Solid State Phys.* **19** 7013
[18] Herring C and Kittel C 1951 *Phys. Rev.* **81** 869
[19] Rado G T and Weertman J R 1959 *J. Phys. Chem. Solids* **11** 315
[20] Landau L and Lifshitz E 1935 *Phys. Z. Sowjetunion* **8** 153
[21] Jorzick J, Demokritov S O, Hillebrands B, Berkov D, Gorn N L, Guslienko K and Slavin A N 2002 *Phys. Rev. Lett.* **88** 047204
[22] Park J P, Eames P, Engebretson D M, Berezovsky J and Crowell P A 2003 *Phys. Rev. Lett.* **89** 277201
[23] Bayer C, Demokritov S O, Hillebrands B and Slavin A N 2003 *Appl. Phys. Lett.* **82** 607
[24] Mathieu C, Jorzick J, Frank A, Demokritov S O, Hillebrands B, Bartenlian B, Chappert C, Decanini D, Rousseaux F and Cambril E 1998 *Phys. Rev. Lett.* **81** 3968
[25] Jorzick J, Demokritov S O, Mathieu C, Hillebrands B, Bartenlian B, Chappert C, Rousseaux F and Slavin A N 1999 *Phys. Rev.* B **60** 15194
[26] Demokritov S O, Hillebrands B and Slavin A N 2001 *Phys. Rep.* **348** 441
[27] Landau L D and Lifshitz E M 1960 *Electrodynamics of Continuous Media* (Oxford: Pergamon)
[28] Sandercock J R 1982 *Trends in Brillouin Scattering: Studies of Opaque Materials, Supported Films, and Central Modes* (*Light Scattering in Solids* vol 3) ed M Cardona and G Güntherodt (Berlin: Springer)
[29] Hillebrands B 1999 *Rev. Sci. Instrum.* **70** 1589
[30] Bauer M, Büttner O, Demokritov S O, Hillebrands B, Grimalsky V, Rapoport Yu and Slavin A N 2001 *Phys. Rev. Lett.* **81** 3769

[31] Demokritov S O and Hillebrands B 1999 *J. Magn. Magn. Mater.* **200** 706
[32] Guslienko K Yu and Slavin A N 2002 *Phys. Rev.* B **66** 132402
[33] Joseph R I and Schlömann E 1965 *J. Appl. Phys.* **36** 1579
[34] Bryant P and Suhl H 1989 *Appl. Phys. Lett.* **54** 2224
[35] Schlömann E and Joseph R I 1964 *J. Appl. Phys.* **35** 167
[36] Garcia-Palacios J L and Lazaro F J 1998 *Phys. Rev.* B **58** 14937
[37] Brown W F Jr 1963 *Phys. Rev.* **130** 1677
[38] Braun H-B 2000 Stochastic magnetization dynamics in magnetic nano-structures: from Neél–Brown to soliton–antisoliton creation *Structure and Dynamics of Heterogeneous Systems* ed P Entel and D Wolf (Singapore: World Scientific)
[39] Brown G, Novotny M A and Rikvold P A 2001 *Phys. Rev.* B **64** 134422
[40] Kittel C 1958 *Phys. Rev.* **110** 1295